Astronomy & Astrophysics

Production and kinematics of CO in comet C/1995 O1 (Hale-Bopp) at large post-perihelion distances[*]

M. Gunnarsson[1], D. Bockelée-Morvan[2], A. Winnberg[3], H. Rickman[1], J. Crovisier[2], N. Biver[4], P. Colom[2], J. K. Davies[5], D. Despois[6], F. Henry[2], L. E. B. Johansson[3], R. Moreno[7], G. Paubert[8], and F. T. Rantakyrö[9,10]

[1] Astronomiska Observatoriet, Box 515, 75120 Uppsala, Sweden
[2] Observatoire de Paris, 92195 Meudon, France
[3] Onsala Space Observatory, Sweden
[4] European Space Agency, ESTEC Sci-So, Noordwijk, The Netherlands
[5] Joint Astronomy Centre, Hilo, HI, USA
[6] Observatoire de Bordeaux, France
[7] Institut de Radio Astronomie Millimétrique, Grenoble, France
[8] Institut de Radio Astronomie Millimétrique, Granada, Spain
[9] European Southern Observatory, Casilla 19001, Santiago 19, Chile
[10] Observatorio Cerro Calan, Universidad de Chile, Santiago, Chile

Abstract. Radio observations of different molecular species in comet C/1995 O1(Hale-Bopp) have been carried out regularly since August 1995. We present an analysis of carbon monoxide spectra observed at SEST. A detailed picture of the nature of the post-perihelion outgassing at large heliocentric distances is shown. The data starts at 2.9 AU, with active water sublimation, and stretch outside 10 AU, where CO-driven activity is still detected. The activity is studied using a coma model which separates the outgassing into two different sources, one insolation-dependent source, peaking at the subsolar point, and one isotropically outgassing source. Gas velocities and production rates of the two sources are derived for two different cases. In the first case the isotropic source is assumed to be inside the nucleus, and in the second case this source is assumed to be CO-rich material in the coma. Under both assumptions, the results indicate that the two component sources evolve independently. At heliocentric distances around 3 AU, acceleration of the CO molecules in the innermost region of the coma is required for the model to fit the observations. This acceleration must occur at a slower rate than that predicted by hydrodynamic simulations. From 6 to 10 AU, the derived parameters appear remarkably constant. The nuclear outgassing velocity is generally unchanged with heliocentric distance during this wide interval. Observations of molecules other than CO are included in the SEST dataset, and a comparison is made to the modelling results. HCN and CH_3OH show signs of being produced in the same way as the CO up to a heliocentric distance of 6 AU.

Key words. comets: individual: C/1995 O1 (Hale-Bopp) – radio lines: solar system

1. Introduction

Since August 1995 the outgassing of comet C/1995 O1(Hale-Bopp) has been studied at millimetre wavelengths in an international collaboration using the IRAM[1], JCMT[2], CSO[3] and SEST[4] radio telescopes. Of the eight different molecules monitored in this program, carbon monoxide was the first one to be detected (Biver et al. 1996; Jewitt et al. 1996). Using all of

[*] Based on results collected at the European Southern Observatory, La Silla, Chile.

[1] Institut de Radioastronomie Millimetrique 30-m telescope at Pico Veleta, Spain and interferometer at Plateau de Bure, France.

[2] James Clerk Maxwell Telescope, Mauna Kea, Hawaii, USA.

[3] Caltech Submillimeter Observatory, Mauna Kea, Hawaii, USA.

[4] Swedish-ESO Submillimetre Telescope, La Silla, Chile.

the available data, general power-laws have been derived from basic line parameters for the expansion velocity, kinetic temperature and production rates of the different molecules (Biver et al. 1997, 1999).

As CO has been detected over a very wide range of heliocentric distances, and generally displays spectra with good signal-to-noise ratios, this is the primary molecule to study in order to determine the outgassing mechanism of the comet as it has changed in character. The present work examines in more detail the spectral features of the CO(2–1) emission line from the SEST dataset, covering the post-perihelion branch from a heliocentric distance, r_h, of 2.9 AU and outward up to 11 AU. CO has been detected also outside 11 AU, but at a level too low for application of the analysis described here.

Comet Hale-Bopp has displayed similarities to the peculiar comet 29P/Schwassmann-Wachmann 1 (hereafter SW1).

These two comets both have large nuclei, although different values have been estimated for the diameter of SW1. A diameter roughly equal to that of comet Hale-Bopp was found by Cruikshank & Brown (1983), while about half of this value was found by Meech et al. (1993). Emission from CO molecules in SW1 was first detected through the $J = 2$–1 transition in 1993 (Senay & Jewitt 1994). Observations in the following year (Crovisier et al. 1995) revealed the shape of the emission line. The line has a strongly asymmetric profile with a blueshifted peak, which is a signature of outgassing occurring mostly toward the Sun. For heliocentric distances greater than ~4, the CO emission line in comet Hale-Bopp has a similar signature (Biver et al. 1997). This similarity is strongest for the post-perihelion data, which is examined here. In addition to the blueshifted main peak indicative of CO molecules travelling toward the Sun, a redshifted plateau, or secondary peak, is present in the profile, indicating the existence of molecules moving also in the opposite direction.

The similarity between the two comets, albeit with radically different orbital and thermal histories, is used as a starting point of this investigation. Outgassing models originally developed to study SW1 are employed here to investigate the CO production in comet Hale-Bopp.

For the observations discussed here, with the comet at large heliocentric distances, there are three different CO sources that can be considered: (1) CO is released deep inside the porous nucleus when amorphous water ice crystallizes, releasing volatile species that was initially trapped in the ice (Tancredi et al. 1994; Prialnik 1997; Enzian 1999). As it is expelled into the coma, this gas will have a temperature (and corresponding velocity) equal to that of the nuclear surface, but the amount of gas released will be insensitive to the conditions at the surface. (2) CO is released from exposed ice at the surface, or from a crystallization front residing close to the surface. The production rate is then dependent on the surface temperature, and is expected to peak at the subsolar point. (3) CO is released from icy grains in the coma. The extent of such a source is dependent on the lifetime of the grains. Submicrometre-sized grains sublimate quickly even at large r_h, while larger grains could result in a CO source residing in a large cloud. Source (2)+(3), but with the crystallization front residing close to the nuclear surface, is the mechanism assumed to be at play in comet SW1 (Gunnarsson et al. 2002).

In the present work, all three of the above sources are discussed and their relative contributions to the total CO production are derived.

The comet is now at a distance where it is very hard to detect, marking the end of the long Hale-Bopp radio observing campaign. The final observations were done in January 2002, at $r_h = 15$ AU. A summary of the campaign is presented in Biver et al. (2002). Other papers that will present the wealth of collected data are also in preparation.

2. Observations

Observations of Hale-Bopp have been carried out at SEST on a regular basis, with an observing run almost every month since September 1997. The dates of observation are listed in Table 1.

Of the molecules observed, e.g. HCN, CH_3OH and H_2S, only carbon monoxide is detected since September 1998. This molecule is detected in the $J = 2{\rightarrow}1$ rotational transition (rest frequency 230.538 GHz). The SEST has a 15 m diameter paraboloid reflector with a half-power beamwidth of 22″ and a beam efficiency of ~50% at this frequency. The telescope has a front-end receiver based on a liquid helium-cooled SIS mixer and a backend consisting of an acousto-optical spectrometer. The tracking of the comet was controlled by an ephemeris computed using *Horizons*, provided by JPL (Giorgini et al. 1996, see ssd.jpl.nasa.gov/horizons.html).

At the start of the SEST observations several molecules were detectable and CO was observed during a part of the allocated time only. Later on, when CO became the only detectable species, it has been integrated for complete observing runs, spanning several days. Because of this the later observations represent more of a time-average picture of the outgassing pattern, while the earlier are more like "snapshots", more sensitive to activity variations possible in the case of a heterogeneous nuclear surface, considering the observed rotational period of 11.4 h (e.g. Jorda et al. 1999). The first column in Table 1 show only the dates when CO was observed.

3. Modelling

The aim of the modelling is to treat the observed CO spectra as the sum of contributions from CO sources of different nature, to distinguish between them and to compare, primarily, the corresponding production rates of these sources. Some basic principles of the outgassing pattern have to be set up, and this pattern must be controlled by a limited set of model parameters. The output of the model is a simulated emission line profile that can be directly compared to the observational data. The goal is to keep the model assumptions and parameters for the outgassing pattern as simple as possible, while the model calculations must take all processes into account, that influence the signal detected by the telescope receiver. To obtain an accurate simulation the model calculates the influence of the changing population of the rotational levels of the molecules, the photodissociation lifetime and the antenna response profile.

Modelling of this nature has been done for comet SW1 using Monte Carlo simulations (Festou et al. 2000; Gunnarsson et al. 2002). Because of the striking similarity of the CO(2–1) emission line profile of SW1 and Hale-Bopp when the latter moved outside $r_h = 6$ AU, those models are employed here for the Hale-Bopp data as well. Two different approaches for modelling the outgassing pattern are investigated.

In the first, only nuclear outgassing is assumed. This view allows activity over all of the nuclear surface. The outgassing velocity is dependent on the energy received from insolation. Two component sources, corresponding to case (1) and (2) in Sect. 1, contribute to the outgassing, and the local production rate is thus partly dependent on location on the nuclear surface.

In the second approach, nuclear outgassing is present on the dayside of the nucleus only. A secondary source of CO is present, consisting of icy grains released together with the dayside outgassing, moving with a fraction of the CO velocity. These grains in turn produce CO, which is released

isotropically around each grain. These sources represent case (2) and (3) in Sect. 1.

The model generates an artificial line profile to be compared to the observed spectra. To evaluate the chosen model parameters, the quality of the model fit is studied by subtracting the simulated spectrum from the observational data in order to give a "difference signal". When the level of this difference is equal to or below the surrounding noise fluctuations the fit cannot be reliably improved. Therefore the S/N ratio of the observational data is a crucial item when determining the model parameters. Fortunately most of the CO spectra contain much detail above the noise for an accurate fit to be done.

3.1. Model considerations

Since the CO $J = 2$–1 line is observed, the relative population of the rotational $J = 2$ level is an important factor to include in the calculations. A model for the evolution of the rotational population after release of the molecules is used. The molecules are assumed to be excited through both collisional and radiative processes.

Collisional self-excitation of CO, as well as excitation by collisions with H_2O which dominates at $r_h < 4$ AU, must be included. The H_2O production rate, as a function of heliocentric distance, is estimated from the observed rates (Biver et al. 2002). The cross-sections for collisional re-arranging of the rotational levels are not well known. For CO–CO collisions, the value adopted here is $\sigma_c(\text{CO–CO}) = 2 \times 10^{-14}$ cm^2 (Biver 1997). For CO–H_2O collisions, one published value of σ_c(CO–H_2O) is 1.32×10^{-14} cm^2 (Chin & Weaver 1984), and the calculations described by Green (1993) lead to values in the range 1.1–1.2×10^{-14} cm^2 for temperatures under 100 K. A value of 1.2×10^{-14} cm^2 is adopted here. However, the uncertainty in this value does not have a significant effect on the calculated emission line.

The radiative excitation is governed by infrared pumping of the vibrational $v = 0$–1 band. A cometocentric radius r_e is used to define the point where the total collisional and radiative excitation rates are equal. In order to calculate r_e, estimates are needed for the total production rates and expansion velocity. These are given in a compact way as exponential functions, proportional to r_h^{-x}, by Biver et al. (1999). The dependence of r_e on r_h is shown in Fig. 1. The 11″ half-power beam radius of the SEST is included for comparison. The observed part of the coma is dominated by collisions at the beginning of the SEST observations, but outside ~5 AU collisions govern the excitation only at the centre of the beam. The initial distribution established here is subject to a slow change when radiative pumping changes the population of the rotational levels toward fluorescence equilibrium as the molecules travel outward. The excitation model used is described in Gunnarsson et al. (2002). This model provides the coma model with an approximation of the time-dependent excitation, expressed as a compact analytical function. The difference between this approximation and a detailed modelling run is small. It is accurate enough for use in the present application, because of the averaging nature of the
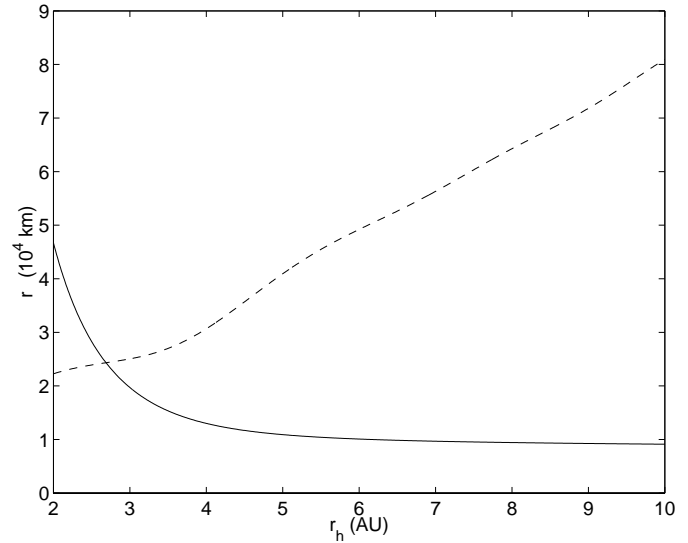

Fig. 1. The radius of equal collisional and radiative excitation rates r_e (solid), compared to the beam radius at the distance of the comet (dashed), both as a function of heliocentric distance.

coma model, where the emission from each molecule is integrated over time.

The first modelling approach uses the same form for the outgassing pattern as that which was derived from the line profile of SW1 from the 1996 observations at SEST (Festou et al. 2000). Here the expansion velocity and local production rate are given by continuous functions of $\mu = \max(\cos(\theta), 0)$ where θ is the solar zenith distance as seen from the nuclear surface. The local production rate q has the form

$$q \propto (\mu^2 + c) \tag{1}$$

where c is a numerical constant. This is a compact way of describing a combination of the insolation-dependent and isotropic sources (1) and (2) discussed above, with c controlling the relative contribution of the latter. The local production rates of the two sources can be separately written as $q_d \propto \mu^2$ and $q_n \propto c$, and the corresponding total rates are hereafter denoted Q_d and Q_n. The expansion velocity is given by

$$v_{\exp} = (v_s - v_n)\mu + v_n \tag{2}$$

where v_s is the velocity at the subsolar point. It is thus assumed to be constant ($= v_n$) over the night side. Together with a kinetic temperature T_k which controls the rotational population in the collision zone and the broadening of the line, this modelling approach defines the outgassing pattern with a small set of model parameters, characterized by outgassing coming entirely from the nucleus, and with activity present on the nuclear nightside.

The second modelling approach was also derived from SW1 observations, and takes CO production from a non-nuclear source into account. This was necessary to fully explain all SW1 observations done at SEST, which includes lines recorded at spatially offset locations. Here the nuclear outgassing is restricted to the dayside, varying as

$$q \propto \mu^2. \tag{3}$$

The agent of the secondary source is assumed to be icy grains that follow the nuclear CO outflow with a fraction of its velocity. These grains also produce CO which isotropically escapes the rest frame of each grain with a given velocity distribution. The emission line profile generated by the model is thus a superposition of two lines, one blue-shifted from the nuclear source, and one extending to both the red and blue sides from the secondary source. The model parameters are:

v_s Nuclear CO outgassing velocity (m s^{-1}), taken to be the same as in the previous scenario.

η_{vel} Fraction of the nuclear CO outgassing velocity, acquired by the grains.

T_k Kinetic temperature in the innermost coma, nuclear source (K).

T_e Kinetic temperature of CO produced in the secondary source (K).

Q_d Total production rate, nuclear (dayside) source (Molecules s^{-1}).

Q_e Total production rate, secondary source (Molecules s^{-1}).

In both models, the model fitting procedure is done by first setting the value of v_s, to give the blueshifted narrow peak its correct velocity. T_k is adjusted to fit the slope of the blueshifted edge of the line. These two parameters can be very accurately fit since they describe the dominating feature of the line. For the nuclear outgassing model, the nightside velocity, v_n, is then set to fit the red edge of the line. The corresponding adjustment in the extended source model is influenced by all parameters describing the outgassing from grains.

Since the grains in the extended source are assumed to produce their CO at some distance from the nucleus, where the coma is very thin in comparison, this gas does not go through the adiabatic cooling that the nuclear CO does, and the temperature of this gas should thus be that of the grains. In all model runs this temperature, T_e, was set to 150 K, just below the sublimation point of water ice. Trapped CO in the ice that was not released at crystallization will evaporate together with the H$_2$O ice (Bar-Nun & Kleinfeld 1989). However, in order to get a fit it has been shown (Gunnarsson et al. 2002) that a small velocity increment v_e must be added to the CO from grains, resulting in a slightly distorted gaussian distribution. This addition is necessary for the model line to cover the velocity range seen in the observed spectra, and appears unavoidable for both SW1 and Hale-Bopp. Simply increasing the temperature to get higher velocities leads to unrealistic values (~300 K) and does not give the right line shape.

Finally, the values of Q_d and Q_n, or Q_d and Q_e, are determined using an automatic least-squares method. This process is reiterated until an optimal fit to the data is achieved.

In the extended source model, the grains are assumed to produce CO outside the collision-dominated coma, making it possible for these molecules to travel in the same direction as the nuclear outgassing, but with a different velocity. In some of the spectra, this ingredient makes it possible to attain a better fit to the data near zero velocity than in the nuclear outgassing model. The release of CO from grains is naturally thought to
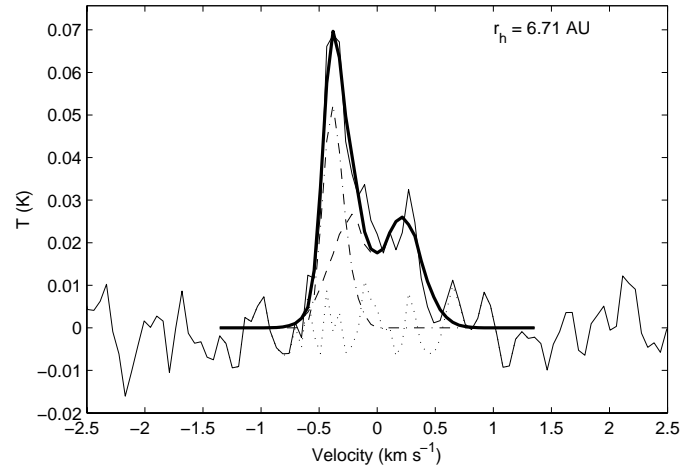

Fig. 2. Example of how the extended source model produces a fit (thick line) to the observed line (thin) from the nuclear (dashed-dotted) and secondary (dashed) components.

occur at some distance from the nucleus. This distance could be the result of a time delay connected to a slow heating process before the bulk of the CO-bearing grains start sublimating. For the source to actually show an observably extended nature, as in the case of SW1 for which a spectral mapping was done (Gunnarsson et al. 2002), this distance must be large, comparable to around two times the projection of the beam diameter. However, no offset observations were done for comet Hale-Bopp, and thus no information is available about the extent of this source. It is consequently set to occur near the nucleus (albeit outside the collision zone), and the derived value of its production rate is therefore a minimum value, since a greater extent would cause more molecules to be lost outside the beam, thus requiring a higher production rate.

Spectra recorded with the comet inside a heliocentric distance of 3.8 AU constitute a special case, since water sublimation is active. If the extended source is active here, it cannot be distinguished from nuclear outgassing since the lifetime of icy grains should be very short. Furthermore, the production region of CO was shown to have no extent at 2 AU using high resolution infrared spectroscopy (DiSanti et al. 1999; DiSanti et al. 2001). Inside 3.8 AU the observed spectra lack the sharp "horned" characteristic expected from simple outgassing models. This is assumed to be due an increasing expansion velocity which makes the line profile broader as the gas molecules contributing to it have a range of velocities rather than a single velocity. To allow for this effect, the first three SEST spectra are treated separately in Sect. 3.3.

3.2. Model fits

For all spectra outside 3.8 AU, which appears to be the turn-off point for H$_2$O sublimation (Biver et al. 1999), the line has a characteristic shape that retains its basic features over the rest of the dataset, up to above 10 AU. A blueshifted peak dominates the shape, and since the comet is viewed at a small phase angle (decreasing from 15 to 5° during the period discussed here), this peak is readily identified as nuclear outgassing

peaking at the subsolar point. The remainder of the line is a structure extending over both the red- and blueshifted sides, often giving the line a double-peak character. This is referred to here as the isotropic component.

The parameters used for the model are listed in Table 1, together with the values of r_h and Δ when the individual observations were done.

Examples of the model line profiles for the two scenarios, superimposed on the actual spectra, are shown in Figs. 3 and 4. In the spectra recorded below 3.8 AU the line shape is strongly broadened and completely engulfed in the isotropic component. As water sublimation turns off, the line area of the isotropic component decreases steeply, as does its broadening (Figs. 3A and 4A), and a double-peak structure is formed. In the nuclear outgassing case, the model line provides a good fit to most spectra, though in some cases it displays a deeper "dip" near zero velocity than observed.

For the extended source case, the main peak is in most cases a superposition of the nuclear component and one side of the isotropic component. Outside 6 AU the grain velocity, described by η_{vel}, must be small for the model to fit the data. It is set to 0.05 for all spectra outside this r_h, which corresponds to velocities lower than the separation between two channels in the spectrometer. This is thus an uncertain value, and should be seen as an indication that the extended source material is moving at a velocity of no more than 50 m s^{-1}.

Outside 7 AU the height of the blueshifted peak drops, while the remainder of the line maintains an almost constant area (Figs. 3D and 4D), at least up to 10 AU.

Returning to the nuclear outgassing model, the velocities v_s and v_n are seen to follow relatively smooth trends (Fig. 5). Starting at small r_h, these two velocities are decreasing, as the last of the H_2O sublimation disappears. Outside 5 AU, the velocities are then remarkably stable for the remainder of the period, up to 11 AU. The velocities are thus unchanged during a period when the energy received from the Sun drops by a factor of four. It has been possible to follow the evolution of v_s even further, since it is very close to the Doppler shift of the main peak of the emission line, and it has remained at ~400 m s^{-1} up to 14 AU (Biver et al. 2002).

For the extended source case, the small velocity v_e was set to 70 m s^{-1} in most cases in order to get a fit to the data. Higher values for this parameter were necessary at small r_h. This could be an effect of CO being released from grains "early" in the coma. While the model assumes the molecules from grains to be unaffected by the rest of the coma, they may not have left the region where the gas is accelerated, and could thus become slightly faster.

In both outgassing models, the model line profile could be fit to the data in all listed spectra with no residual signal sticking out of the surrounding noise level.

3.3. Modelling at low r_h

For CO-dominated comets (outside ~4 AU) the above simple modelling approaches can be employed, since the region where the CO molecules are accelerated to their terminal velocity is very small compared to the beam radius. The telescope effectively "sees" molecules leaving the nucleus with a single velocity. At lower r_h, where H_2O sublimation is active, the shape of the observed line profile departs from the theoretical "horned" shape expected from a model with a single outflow velocity. The terminal velocity of the molecules can still be deduced from the edges of the line profile, but the region of acceleration has a non-negligible extent compared to the beam. Molecules of a wider range of velocities are included in the data, and the centre part of the line is "filled in", resulting in a broad single peak structure.

To model the line shape in the first three spectra of the dataset, the molecules must thus start out at a smaller velocity, and be accelerated toward their terminal velocity.

Whether or not the CO production has a coma component, the CO production is expected to appear as being nuclear at these r_h. The nuclear outgassing model is thus employed, where an asymmetric outgassing pattern can be modeled, and where the initial outflow velocity is given by (2). The outflow velocity then increases with increasing nucleocentric distance. This acceleration is assumed to follow the formula (Lovell 1999):

$$v = v_{exp} \left(\frac{r}{r_n} \right)^\alpha$$

where α is a dimensionless exponent and r_n the nuclear radius. The coma model, which is described in detail in Gunnarsson et al. (2002), is based on integration of the motion of the molecules over time. The formula is rewritten as a function of t,

$$v = v_{exp} \left(\frac{v_{exp} t (1 - \alpha)}{r_n} + 1 \right)^{\frac{\alpha}{1-\alpha}}$$

and included in the model code.

Values of the model parameters used, including α, are listed in Table 2.

The model profiles compared to the observed spectra are shown in Fig. 6.

While these three line profiles appear as broad, single peaks as opposed to the line shapes encountered at greater r_h, they are still asymmetric. The outgassing velocity and local production rate is higher toward the Sun, and the blueshifted edge of the profile appears at a higher velocity than the redshifted edge. As the gas is accelerated, it is also diluted and makes a smaller impression on the observed line. Because of this, the model predicts a slightly less steep slope on the blueshifted side, an effect that is best seen for spectrum A in Fig. 6. The general result here is that to explain the line shapes, the initial acceleration of the gas must be a gradual process spanning ~10^4 km.

The values of α found from the fitting are very close to that used by Lovell (1999) to explain the line shape of the HCN(1-0) line for Hale-Bopp near perihelion (for March 24, 1997). However, the gas acceleration described by this value of α is not similar to that predicted for Hale-Bopp at $r_h = 3$ AU using hydrodynamic simulation (Combi et al. 1999). In that simulation the acceleration from the initial velocity occurs quickly during the first 100 km, and the velocity then remains at a nearly steady value, with a slow acceleration from photochemical heating. A similar pattern was seen also in modelling by
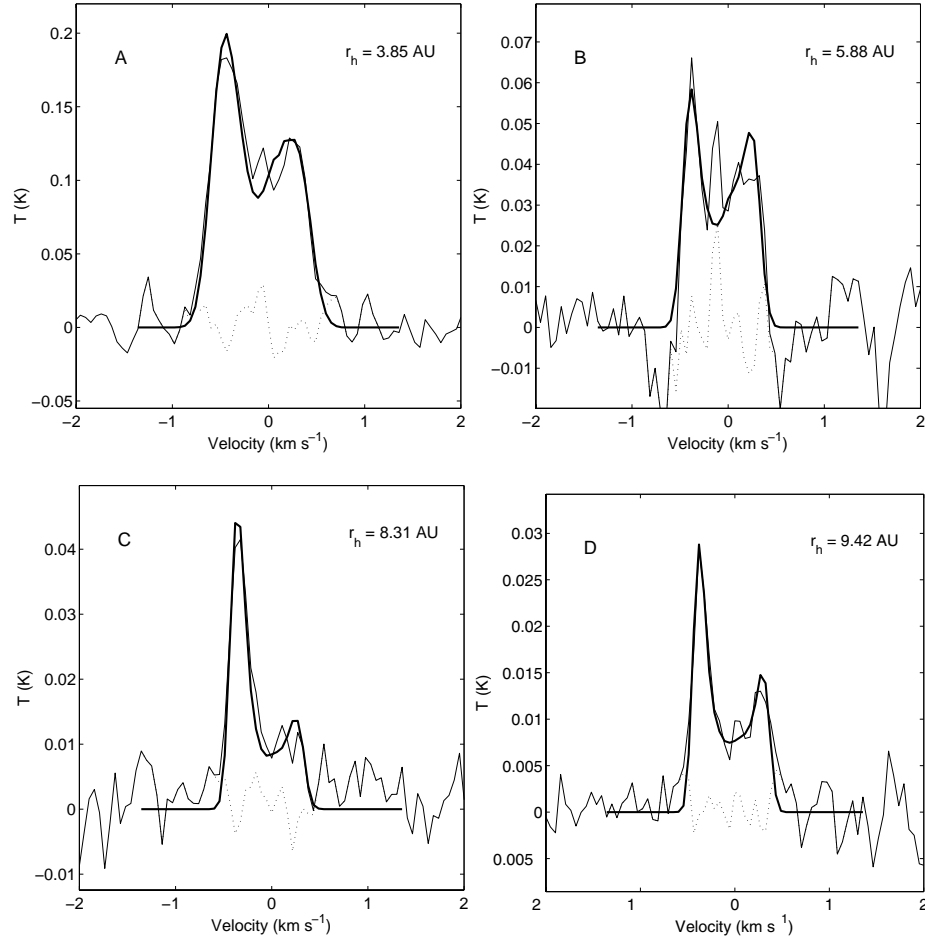
Fig. 3. CO(2–1) spectra at various r_h (thin lines), together with the fitted model profiles (thick lines) using outgassing by a nuclear CO source only. The difference signal (dotted) is also shown. Antenna temperatures are shown. Note the different temperature scales.

Table 1. Parameters used in the model for the different spectra.

Date		Δ	r_h	v_s	T_k	v_n^*	η_{vel}^{**}	v_e^{**}	Q_d^*	Q_n^*	Q_d^{**}	Q_e^{**}
		(AU)	(AU)	(m s^{-1})	(K)	(m s^{-1})		(m s^{-1})	($\times 10^{28}$ s^{-1})	($\times 10^{28}$ s^{-1})	($\times 10^{28}$ s^{-1})	($\times 10^{28}$ s^{-1})
24/12	1997	3.68	3.85	580	30	420	0.10	150	2.16	6.63	1.30	11.54
1/1	1998	3.76	3.93	570	30	450	0.10	150	1.85	4.03	1.61	8.32
26/1–27/1	1998	4.10	4.22	600	25	350	0.20	110	1.98	2.81	1.52	7.03
28/2	1998	4.48	4.50	600	25	280	0.20	90	1.38	1.13	1.14	3.19
18/3–19/3	1998	4.74	4.70	560	25	320	0.10	50	1.97	1.73	1.90	3.50
15/7–20/7	1998	6.06	5.88	450	15	320	0.05	70	0.32	1.26	0.29	2.66
10/8–12/8	1998	6.28	6.13	450	15	320	0.05	70	0.34	0.89	0.30	2.00
15/9	1998	6.52	6.42	450	13	320	0.05	70	0.33	0.86	0.31	1.88
20/10–22/10	1998	6.79	6.73	450	13	330	0.05	70	0.58	0.98	0.56	2.05
15/11–17/11	1998	7.00	6.94	450	13	400	0.05	100	0.38	1.04	0.40	1.94
25/12–31/12	1998	7.35	7.29	420	12	400	0.05	70	0.65	0.78	0.78	1.27
18/1–20/1	1999	7.54	7.48	430	11	320	0.05	70	0.62	0.68	0.61	1.42
7/3–11/3	1999	7.94	7.87	430	11	320	0.05	70	0.34	0.55	0.32	1.22
1/5–5/5	1999	9.14	8.31	410	11	320	0.05	70	0.38	0.48	0.35	1.00
21/9–30/9	1999	9.47	9.42	420	9	350	0.05	70	0.20	0.64	0.23	0.94
8/12–13/12	1999	10.12	9.98	440	8	350	0.05	70	0.15	0.79	0.19	1.03
7/1–19/5	2000	10.79	10.75	440	8	350	0.05	70	0.27	0.44	0.26	0.76

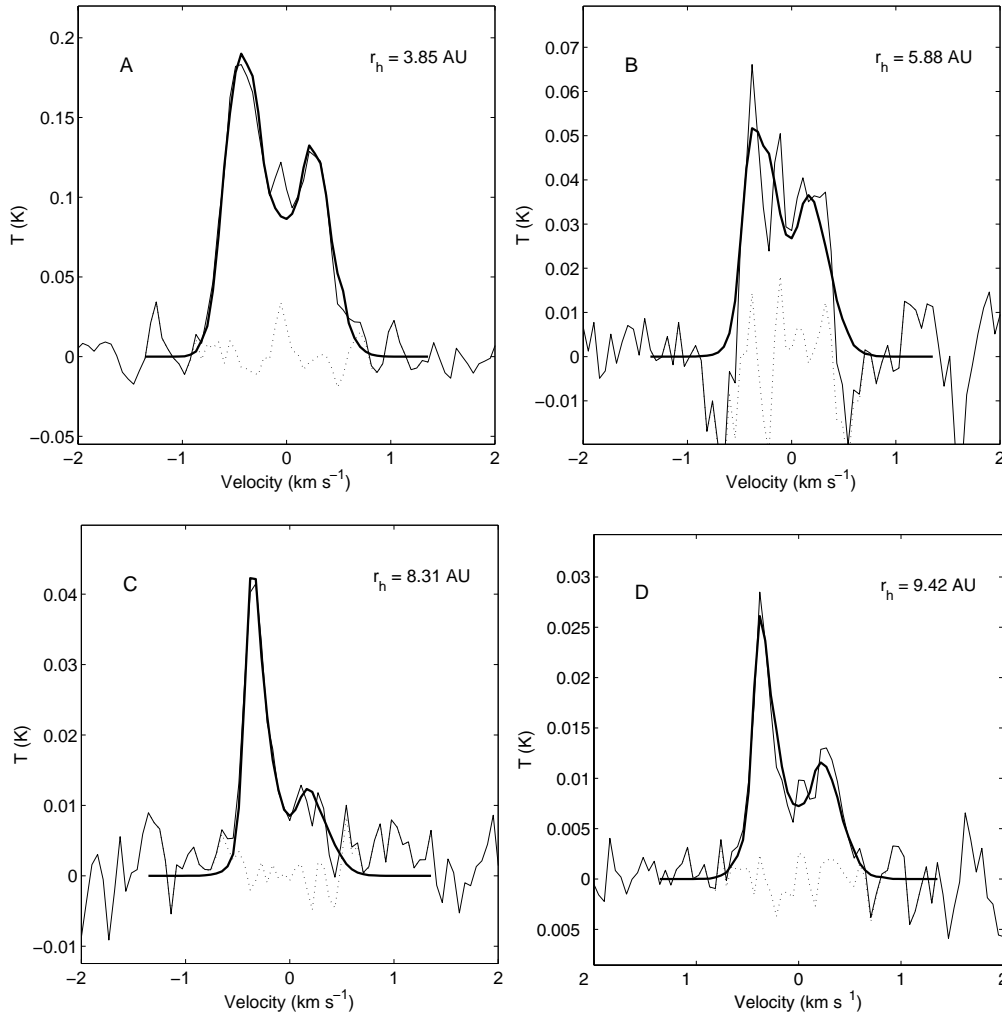* For the nuclear outgassing case.

** For the extended source case.

Fig. 4. The same CO(2–1) spectra as shown in Fig. 3 (thin lines), together with the fitted model profiles (thick lines) using the assumption of an extended CO source.

Ip (1983) for comets at 1 AU from the Sun, both for a CO coma and a CO-H_2O mixture.

3.4. CO production rates

For most of the observed spectra, the S/N ratio is good enough for the model parameters used to be regarded as observed, rather than being chosen ad hoc. The main result is the relative production rates of the contributing sources. The production rate of dayside CO outgassing (Figs. 7 and 8) displays a general adherence to a curve proportional to r_h^{-2}, except for a dip at 6 AU. Apparently, the dayside CO outgassing is not influenced by the presence of water sublimation below 4 AU. The production rate of the isotropic component, however, displays a clear relationship to the water sublimation. Inside ~4.5 AU this production rate is much greater than the dayside rate, and shows a steep decrease. Surprisingly, outside 9 AU an increase is seen in the production rate of this component, making it markedly stronger than the dayside source and giving a general impression that it remains roughly constant from 5 to 10 AU, an interval in which the energy received from the Sun decreases by a factor of four. The error bars shown are calculated for each
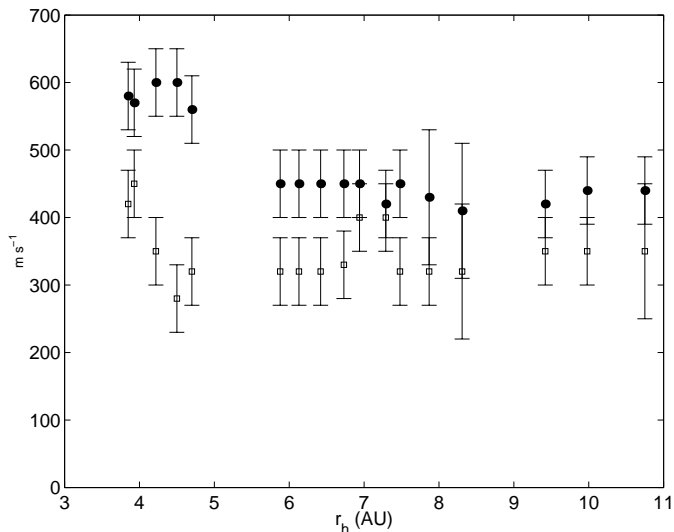
spectrum as $\pm 1\sigma$ compared to the partial line areas of the dayside and secondary components respectively. The kinetic temperature T_k found here agrees well with the power law derived by Biver et al. (1999), which is based both on observed line widths and the relative strength of different lines closer to the sun. An exception is the values at $r_h \simeq 3.8$ AU, where a slightly higher temperature is required to get the observed line shape. It is assumed that this extra broadening is an effect of the acceleration that was treated separately in Sect. 3.3, which influences also this line to some degree.

Our total (day+night) production rates in the nuclear outgassing model are on average 40% lower than those published by Biver et al. (1999, 2002), from the same set of data. The difference comes mainly from the fact that the latter production rates are computed under the assumption of completely isotropic CO outgassing.

The extended source model (Fig. 8) requires a higher production rate from grains than in the isotropic component in the nuclear outgassing case, because of the relatively hotter gas released from grains which initially populate higher J levels. For both models, the two component sources appear to be independent of each other over time, indicating that they are

Table 2. Parameters used in the model for the three lowest r_h.

Date		Δ (AU)	r_h (AU)	v_s (m s^{-1})	v_n^*	T_k (K)	α	Q_d (×10^{28})	Q_n (×10^{28})
28/9	1997	3.10	2.87	240	170	30	0.16	2.5	12.8
9/10	1997	3.13	2.97	240	170	30	0.14	2.2	5.4
28/10	1997	3.23	3.23	240	160	30	0.14	2.0	6.2

Fig. 5. Velocities used in the nuclear outgassing model. Filled circles denote the subsolar outgassing velocity v_s and the squares show the outgassing velocity of the isotropic component source, v_n. For most spectra, the error bars are dominated by the uncertainty in velocity tracking induced by the instrumentation, typically $\pm \sim 50$ m s^{-1}.

indeed of different nature. In the extended source case, the production rate of the extended component follows a smoother trend than the nuclear component. A slowly dispersing cloud of grains, where individual grains could remain inside the beam for weeks, would filter out temporal variations in nuclear output, which do show up when observing gas molecules coming from the nucleus.

3.5. Other molecules

Aside from carbon monoxide, emission lines of numerous other molecules were recorded during the observing campaign. HCN and CH$_3$OH were detected at a heliocentric distance as large as 6.1 AU. These observations are to be published in detail elsewhere (Biver et al. 2002; Bockelée-Morvan et al., in prep.) We discuss here some of these spectra which have a S/N ratio good enough to enable a direct comparison with the CO line profiles. The different molecules are all excited and emitting through different quantum transitions, and observed with different beamwidths, but the general shape of the lines and the velocity channels covered by the profile can be directly compared. The H$_2$S(1_{10}–1_{01}) line at 169 GHz has sharply defined edges and is symmetric around zero velocity, whereas the CO line is always asymmetric in the observations presented here, having its negative velocity edge at a greater velocity than the positive edge. H$_2$S was detected at 3.9 AU, the smallest r_h

where the extended source model is applied. Figure 9 (top) shows a comparison of the H$_2$S line to the two component lines derived from the CO line in the extended source model. A correspondence to the secondary component is seen, both in the velocity interval covered and the symmetric shape of the line, indicating that the release of this molecule could be associated mostly to the secondary, extended source. When comparing these lines, it should be pointed out that H$_2$S is not efficiently excited by IR pumping at this r_h, which gives this molecule a smaller emission region than that of CO. If H$_2$S is produced by a nuclear source the line shape would also be expected to be different from CO. Yet, because of the symmetry of the line, release of H$_2$S appears to be connected primarily to the isotropic component in both the nuclear and extended source cases.

In the subsequent observation (at 3.93 AU) the H$_2$S line area was very weak and this species was not followed further.

The lower frequency of the HCN($J = 1$–0, $F = 2$–1) emission line (89 GHz) gives a lesser velocity resolution than for CO, but the velocities covered, and the asymmetric shape of this line generally agrees with that of CO.

The CH$_3$OH lines at 145 GHz also display shapes that do not differ significantly from the CO lines. Figure 9, bottom, shows a comparison between the modeled CO line and its two components, and the observed CH$_3$OH 3_0–2_0 A^+ line at 145.103 GHz (the modeled line is adjusted by a factor of 2 in temperature).

The agreement which is seen seen for both HCN and CH$_3$OH at these r_h indicates that the processes that release CO also govern the production of these molecules, up to 6.1 AU, after which they have not been detected. A similar comparison was done on the pre-perihelion branch by Biver et al. (1997). In that work the shapes of the CO and CH$_3$OH lines were reduced to a net Doppler shift of the lines. This Doppler shift was similar for the two molecules between 2 and 4 AU, but different at greater r_h. At 5 AU pre-perihelion, the doppler shift was nearly 0 for CH$_3$OH, i.e. a symmetric line around the nuclear rest velocity. This was observed also by Womack et al. (1997) using the NRAO 12-m telescope on Kitt Peak, Arizona, USA. The interpretation of this could be that the secondary source of this molecule turned on earlier than the nuclear source, but that there was no such difference post-perihelion.

4. Discussion

In addition to the three CO production mechanisms mentioned in Sect. 1 two more should be mentioned here. The first is the photodissociation of a known parent molecule. This process indeed results in an extended CO source, but the candidates are limited. CO$_2$ and CH$_3$OH form CO, but their photodissociation
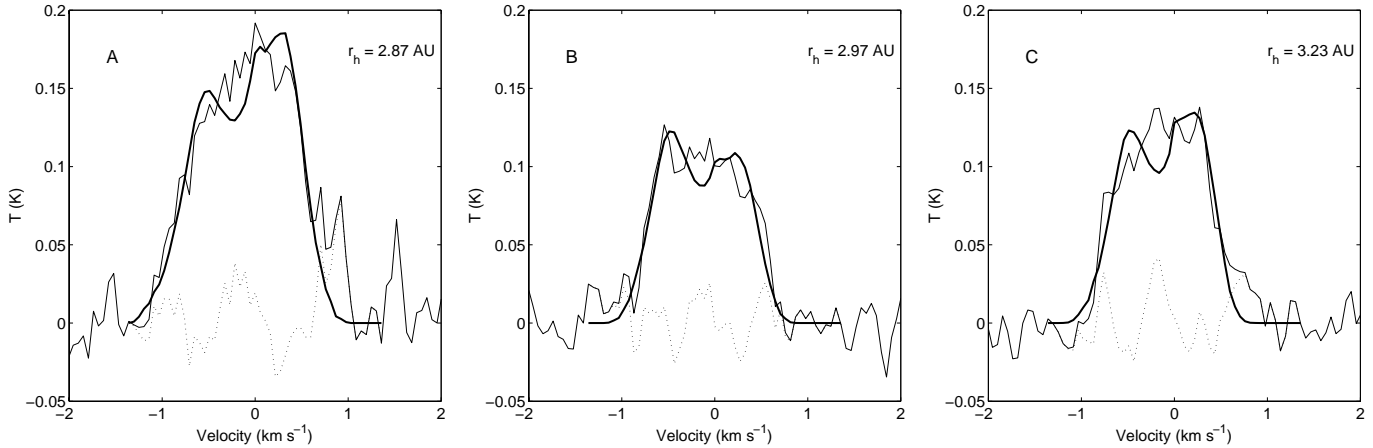
Fig. 6. Model profiles (thick lines) compared to the three observed spectra (thin lines) with smallest r_h, where acceleration of the CO molecules is included in the model.

lifetimes are too long to produce an extended source like that discussed here. H_2CO has the right lifetime to fit the requirements (Meier et al. 1993), but this molecule is not available in sufficient amounts in Hale-Bopp, since its production rate was observed to drop rapidly already at $r_h = 3$ AU (Biver et al. 1999). The second process is the extended CO source observed at small r_h in both comet 1P/Halley (Eberhardt et al. 1987) and Hale-Bopp (DiSanti et al. 1999) when at 1 AU from the Sun. What constitutes this source is still mysterious, but a possible explanation could be CO released by photolysis or pyrolysis of organic mantles on refractory cometary grains (Crovisier 1999). Such a process could only occur close to the Sun, and in Hale-Bopp, it was indeed observed to turn off at $r_h = 2$ AU.

Two possible CO production scenarios are presented here, and modelling using both approaches can produce fits to the observed spectra. Both models also present some difficulties.

For the nuclear outgassing model, Fig. 7 shows that from 6 to above 11 AU the dayside source is declining with heliocentric distance, while the isotropic source becomes markedly stronger outside 9 AU. The isotropic source is assumed to be the interface between crystalline and amorphous ice, and for the above phenomenon to occur, strong variations in this source must be possible. At the same time it must be residing deep enough not to be quickly influenced by the decreasing surface temperature as the comet moves away from the sun.

Below 4.5 AU, water sublimation is active, a process which erodes the surface layers of the nucleus. The dayside source, which is assumed to be close to the surface, should be expected to show some correlation to the gradual disappearance of water sublimation. Instead, it roughly follows an r_h^{-2} trend. The isotropic source, however, which gives rise to the symmetric part of the emission line, shows a disctinct drop in activity as water sublimation disappears, after which it levels out. This does not agree with the idea that the isotropic part should be a crystallization front residing deep within the nucleus, since it would then be insensitive to the surface processes.

The line profile of Hale-Bopp during this interval has the same appearance as that of SW1. On the assumption that all outgassing is of nuclear origin, the outgassing velocities on the day- and nightsides observed in SW1 have been reproduced by
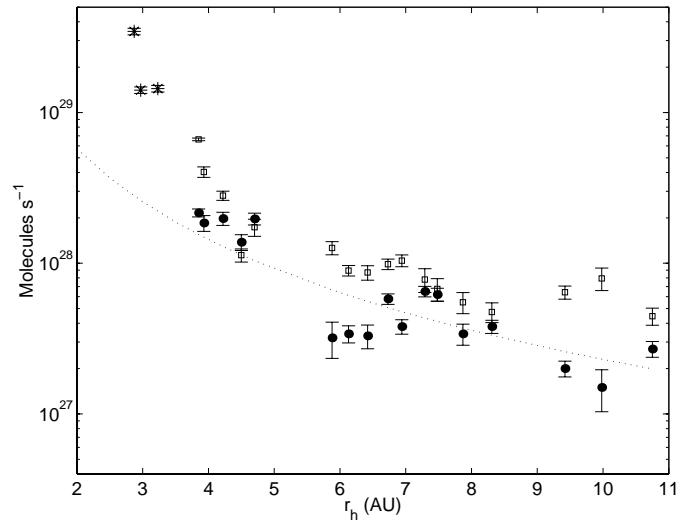

Fig. 7. Evolution of the derived CO production rates in the case on nuclear outgassing as a function of r_h. The dotted line is proportional to r_h^{-2}. Filled circles denote the dayside source and squares the isotropic source. The total production rate derived for small r_h (see Sect. 3.3) is also shown for comparison (asterisks).

hydrodynamic modelling, for a certain nuclear surface temperature distribution (Crifo et al. 1999). Assuming that Hale-Bopp is similar in activity to SW1, it is surprising that the outgassing velocity can remain constant over such a wide range of heliocentric distances as seen here.

For the other scenario, a justification is called for when making the assumption that a part of the CO production in Hale-Bopp originates from an extended source, even at large r_h. The main reason for trying this approach is the previous discovery of an extended source in SW1. However, observations like the CO(2–1) spatial map of the SW1 coma which showed the reality of an extended source have not been performed on Hale-Bopp. It is the similarity in emission line profiles between the two comets (when at $r_h = 6$–7 AU) that leads to the idea that they produce CO in the same way.

The extended source idea fits better to the behaviour below 4.5 AU. Since this idea assumes the isotropic source to be
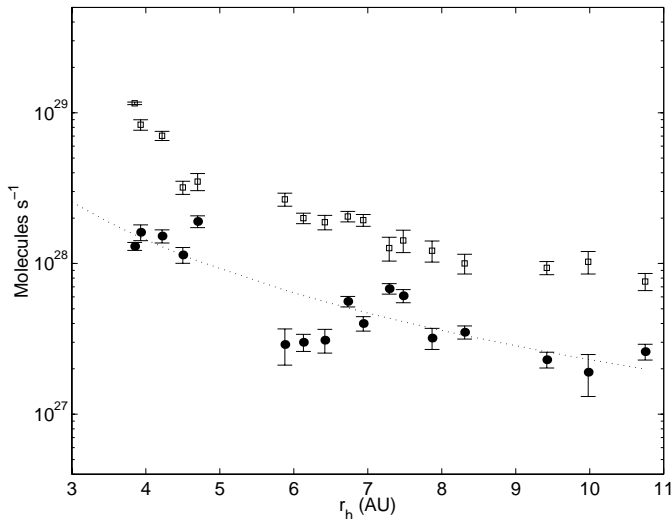
Fig. 8. Evolution of the derived CO production rates in the extended source model. Similarly to Fig. 7 filled circles denote the dayside source. Squares denote the extended source, and the dotted line is proportional to r_h^{-2}.

icy grains, active water sublimation eroding the nuclear surface and releasing such grains could explain the markedly stronger isotropic source seen at these heliocentric distances.

Still, a considerable difficulty with this approach is the high production rate required in the coma source. Very large amounts of solid material must be ejected from the nucleus to sustain such a source. As for the existence – and extent – of a secondary CO source a constraint that must be taken into account is given in the work of DiSanti et al. (1999). They found that the CO production was of nuclear nature when Hale-Bopp was at 2.24 AU post-perihelion, as evidenced by means of long-slit spectroscopy. If part of the CO is produced from icy grains as assumed here, these must exhaust their CO content rapidly after leaving the nucleus at this r_h, making the extent of the secondary source small enough to give the appearance that all CO is coming from the nucleus.

The velocities found for the material constituting the extended source in the model fits are small, below ~ 30 m s^{-1} for $r_h > 6$ AU, to be compared to ~ 100 m s^{-1} observed for $10\,\mu$m grains on the pre-perihelion branch (Fulle et al. 1998). This could be pointing to a different size for the grains mainly constituting the secondary source, or to a change in dust velocity from pre to post-perihelion. In a scenario of grain fragmentation, the slow motion of the active grains could be explained by them being daughter particles of larger grains.

There are several questions to investigate about the reality and nature of an extended secondary source this far from the Sun. Models are needed to study both the nuclear source, which must reside near the surface to give the observed asymmetry in outgassing, and the composition and thermal behavior of the icy grains. Further work in pursuit of an explanation to this is in progress.
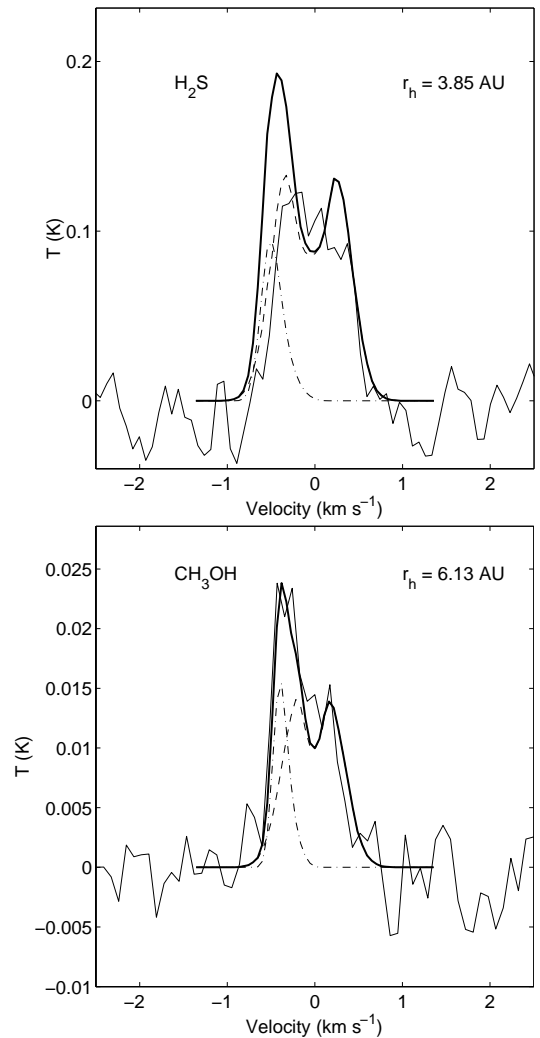
Fig. 9. Observed emissios (thin lines) for the H$_2$S $1_{10}-1_{01}$ line (top) and the CH$_3$OH 3_0-2_0 A^+ line (bottom) compared to the modeled CO J(2–1) lines from the two components in the extended source case. The nuclear and extended components are dash-dotted and dashed lines, respectively. The thick line is the composite modeled CO line. The model line is divided by 2 in the bottom figure.

References

Bar-Nun, A., & Kleinfeld, I. 1989, Icarus, 80, 243

Biver, N. 1997, Ph.D. Thesis, Université Paris VII

Biver, N., Bockelée-Morvan, D., Colom, P., et al. 1997, Science, 275, 1915

Biver, N., Bockelée-Morvan, D., Colom, P., et al. 1999, Earth, Moon and Planets, 78, 5

Biver, N., Bockelée-Morvan, D., Colom, P., et al. 2002, Earth, Moon and Planets, 90, 5

Biver, N., Rauer, H., Despois, D., et al. 1996, Nature, 380, 137

Chin, G., & Weaver, H. 1984, AJ, 285, 858

Combi, M. R., Kabin, K., DeZeeuw, D. L., Gombosi, T. I., & Powell, K. G. 1999, Earth, Moon and Planets, 79, 275

Crifo, J. F., Rodionov, A. V., & Bockelée-Morvan, D. 1999, Icarus, 138, 85

Crovisier, J. 1999, Nature, 399, 640

Crovisier, J., Biver, N., Bockelee-Morvan, D., et al. 1995, Icarus, 115, 213

Cruikshank, D. P., & Brown, R. H. 1983, Icarus, 56, 377

DiSanti, M. A., Mumma, M. J., Russo, N. D., & Magee-Sauer, K. 2001, Icarus, 153, 361

DiSanti, M. A., Mumma, M. J., Russo, N. D., et al. 1999, Nature, 399, 662

Eberhardt, P., Krankowsky, D., Schulte, W., et al. 1987, A&A, 187, 481

Enzian, A. 1999, Space Sci. Rev., 90, 131

Festou, M. C., Gunnarsson, M., Winnberg, A., Rickman, H., & Tancredi, G. 2000, Icarus, 150, 140

Fulle, M., Cremonese, G., & Böhm, C. 1998, ApJ, 116, 1470

Giorgini, J. D., Yeomans, D. K., Chamberlin, A. B., et al. 1996, Bull. Am. Astron. Soc., 28, 1158

Green, S. 1993, ApJ, 412, 436

Gunnarsson, M., Rickman, H., Festou, M. C., Winnberg, A., & Tancredi, G. 2002, Icarus, 157, 309

Ip, W.-H. 1983, ApJ, 264, 726

Jewitt, D., Senay, M., & Matthews, H. E. 1996, Science, 271, 1110

Jorda, L., Rembor, K., Lecacheux, J., et al. 1999, Earth, Moon and Planets, 77, 167

Lovell, A. 1999, Ph.D. Thesis, University of Massachusetts Amherst

Meech, K. J., Belton, M. J. S., Mueller, B. E. A., Dicksion, M. W., & Li, H. R. 1993, AJ, 106, 1222

Meier, R., Eberhardt, P., Krankowsky, D., & Hodges, R. R. 1993, A&A, 277, 677

Prialnik, D. 1997, Earth, Moon and Planets, 77, 223

Senay, M. C., & Jewitt, D. 1994, Nature, 371, 229

Tancredi, G., Rickman, H., & Greenberg, J. M. 1994, A&A, 286, 659

Womack, M., Festou, M. C., & Stern, S. A. 1997, AJ, 114, 2789